Published paper

Boynton, R.J, Balikhin, M.A, Billings, S.A, Reeves, G.D, Ganushkina, N, Gedalin, M, Amariutei, O.A, Borovsky, J.E and Walker, S.N (2013) *The analysis of electron fluxes at geosynchronous orbit employing a NARMAX approach.* Journal of Geophysical Research: Space Physics (118). pp. 1500-1513.

JOURNAL OF GEOPHYSICAL RESEARCH, VOL. ???, XXXX, DOI:10.1029/,

The analysis of electron fluxes at geosynchronous orbit employing a NARMAX approach

R. J. Boynton,[1] M. A. Balikhin,[1] S. A. Billings,[1] G. D. Reeves[2] N. Ganushkina,[3,4] M. Gedalin,[5] O. A. Amariutei,[3] J. E. Borovsky,[6] S. N. Walker[1]

Abstract. The Methodology based on the Error Reduction Ratio (ERR) determines the causal relationship between the input and output for a wide class of nonlinear systems. In the present study, ERR is used to identify the most important solar wind parameters, which control the fluxes of energetic

---

O. A. Amariutei, Finnish Meteorological Institute, Helsinki, Finland. (olga.amariutei@fmi.fi)

M. A. Balikhin, Department of Automatic Control and Systems Engineering, University of Sheffield, Mappin Street, Sheffield S1 3JD, UK. (m.balikhin@sheffield.ac.uk)

S. A. Billings, Department of Automatic Control and Systems Engineering, University of Sheffield, Mappin Street, Sheffield S1 3JD, UK. (s.billings@sheffield.ac.uk)

J. E. Borovsky, Space Science Institute, Boulder, Colorado, USA. (jborovsky@spacescience.org)

R. J. Boynton, Department of Automatic Control and Systems Engineering, University of Sheffield, Mappin Street, Sheffield S1 3JD, UK. (r.boynton@sheffield.ac.uk)

N. Y. Ganushkina, Finnish Meteorological Institute, Helsinki, Finland. (natalia.ganushkina@fmi.fi)

M. Gedalin, Department of Physics, Ben-Gurion University, Beer-Sheva, Israel. (gedalin@bgu.ac.il)

G. D. Reeves, Los Alamos National Labortory, Los Alamos, New Mexico, USA. (reeves@lanl.gov)

S. N. Walker, Department of Automatic Control and Systems Engineering, University of Sheffield, Mappin Street, Sheffield S1 3JD, UK. (simon.walker@sheffield.ac.uk)

[1] Department of Automatic Control and

electrons at geosynchronous orbit. The results show that for lower energies, the fluxes are indeed controlled by the solar wind velocity, as was assumed before. For the lowest energy range studied here (24.1 keV), the solar wind velocity of the current day is the most important control parameter for the current day's electron flux. As the energy increases, the solar wind velocity of the previous day becomes the most important factor. For the higher energy electrons (around 1 MeV), the solar wind velocity registered two days

---

Systems Engineering, University of Sheffield, Sheffield S1 3JD, United Kingdom.

[2] Los Alamos National Labortory, Los Alamos, New Mexico, USA

[3] Finnish Meteorological Institute, Helsinki, Finland

[4] Atmospheric, Oceanic, and Space Sciences Department, University of Michigan, Ann Arbor, Michigan, USA

[5] Department of Physics, Ben-Gurion University, Beer-Sheva, Israel

[6] Space Science Institute, Boulder, Colorado, USA

in the past is the most important controlling parameter. Such a dependence can, perhaps, be explained by either local acceleration processes due to the interaction with plasma waves or by radial diffusion if lower energy electrons possess higher mobility. However, in the case of even higher energies (2.0 MeV), the solar wind density replaces the velocity as the key control parameter. Such a dependence could be a result of solar wind density influence on the dynamics of various waves and pulsations that affect acceleration and loss of relativistic electrons. The study also shows that statistically the variations of daily high energy electron fluxes show little dependence on the daily averaged B_z, daily time duration of the southward IMF and daily integral $\int B_s dt$ (where B_s is the southward component of IMF).

1. Introduction

The region, measured in the equatorial plane, between 1.2 and 7-8 Earth's radii (R_e) is occupied by the terrestrial radiation belts. The configuration of the magnetospheric field in this region, is such that charged particles can be trapped. The radiation belts are filled with energetic electrons with energies from tens of keV up to a few MeV. The slot region, which is located typically between 2-3 R_e, separates the inner and outer radiation belts. While the inner radiation belt is quite stable, the evolution of energetic electron fluxes within the outer radiation belt can be enormous on a very short timescale [*Blake et al.*, 1992; *Reeves*, 1998]. In spite of being discovered during the very first in situ space measurements more than half a century ago [*Van Allen*, 1959], the radiation belts still lack a clear physical model that can be used to explain their dynamics and forecast their evolution under the influence of the solar wind. Since the radiation belts around the Earth and around other planets are very efficient accelerators, understanding the physics involved will advance one of the main fundamental problems of space and astrophysical plasma physics: the mechanisms of particle acceleration in the universe. However, understanding the dynamics of the radiation belts is also very important for modern technological systems, which involve satellites in a low Earth orbit or at geosynchronous orbit. The high fluxes of relativistic electrons significantly increases the probability of the onboard satellite systems malfunctioning and can even result in permanent hardware damage.

While it is widely accepted that the solar wind interaction with the terrestrial magnetosphere and space weather disturbances are related to the dynamics of the radiation belts, this relationship is very complex. This can be illustrated by the relationship between strong magnetic storms and the outer radiation belt fluxes. It was pointed out by *Reeves et al.* [2003] that about half of the magnetic storms lead to a significant increase in electron fluxes, a further quarter result in a decrease in the fluxes and the final quarter of magnetic storms produced no significant change in the fluxes.

A number of physical models have been proposed to explain the dynamics of the radiation belts relativistic electron population [*Friedel et al.*, 2002; *O'Brien et al.*, 2003]. Currently, the most promising models are based on either radial diffusion or local diffusion in the energy/momentum space, resulting from interactions with various waves (e.g. chorus, magnetosonic, etc).

According to the initial models of the radiation belt dynamics, which were based on radial diffusion [*Falthammar*, 1968; *Schulz and Lanzerotti*, 1974], the energization of electrons takes place due to the interactions with electromagnetic fluctuations. These fluctuations result in an earthward diffusion while conserving the magnetic moment and bouncing adiabatic invariant. In the case of a higher phase density, on some outer L shell, diffusion will lead to the integral flow of particles towards the lower L shells. Since the lower L shells will have a higher magnetic field, the electrons must also be energized to conserve the first and second adiabatic invariant. In a number of models, it was suggested that ULF waves could enhance the efficiency of the radial diffusion process [*Rostoker et al.*, 1998; *Elkington et al.*, 1999; *Hudson et al.*, 1999, 2000, 2001].

The second group of models attribute the acceleration of electrons to the interaction with VLF waves in the inner magnetosphere [*Temerin et al.*, 1994; *Shprits et al.*, 2008; *Reeves et al.*, 2009; *Omura et al.*, 2007; *Horne et al.*, 2005; *Summers and Thorne*, 2003; *Summers et al.*, 1998, 2002, 2004; *Albert*, 2003, 2005]. These models assume that the local diffusion in pitch angle and energy space, lead to part of the electron population being lost and another part energized, due to the quasilinear interactions with the generated plasma waves.

A number of recirculation models assume that a combination of radial diffusion and an interaction with ULF waves at low altitude, allow for a fraction of particles to repeatedly undergo a process of Earthward radial diffusion on either a global or local scale [*Fujimoto and Nishida*, 1990; *Liu et al.*, 1999; *Boscher et al.*, 2000]. Other physical mechanisms proposed to explain the build up of a high energy electron population include the Jovian origin of relativistic electrons [*Baker et al.*, 1979] and the penetration of solar wind electrons via the cusp [*Sheldon et al.*, 1998]. These and a number of other ideas are reviewed in *Friedel et al.* [2002].

In addition to the development of models based on first principles, a number of attempts have been made to deduce a forecasting model for the radiation belt electron fluxes directly from data [*Baker et al.*, 1990]. One of the best forecast models was developed by *Li et al.* [2001], however, even this forecast is very far from being perfect.

A number of studies have been devoted to the quest of obtaining the solar wind parameters that control the relativistic electron fluxes in the outer radiation belt. *Paulikas and Blake* [1979] investigated the relationship between electron fluxes and solar wind parameters. The fluxes of > 0.7, > 1.55 and > 3.9 MeV were compared with the solar wind velocity, IMF components and sector polarity for daily averaged, 27 day averaged and 6 months averaged time scales. They concluded that across all these energies, the solar wind velocity exhibits a correlation with the energetic electron fluxes. This conclusion was a landmark result in the study of the radiation belts.

Reeves et al. [2011] have recently conducted a study, investigating the results by *Paulikas and Blake* [1979]. They employed long term data of the daily averaged energetic electron fluxes at geosynchronous orbit and the daily averaged solar wind velocity taken from the OMNI website, for the time period starting on the 22nd September 1989 and ending on the 31st of December 2009. *Reeves et al.* [2011] analysed the relationship between the solar wind velocity and electron fluxes by applying a similar approach to those used in previous studies (e.g. *Paulikas and Blake* [1979]), scatter plots and the Kendall's tau correlation. They found that the relationship between the velocity and electron flux was not the straight forward roughly linear correlation observed by *Paulikas and Blake* [1979]. Instead, *Reeves et al.* [2011] observed a more complex triangular distribution, where on average the higher velocities corresponded to higher fluxes. *Reeves et al.* [2011] results indicates that the fluxes have a velocity dependent lower limit but are independent of the velocity with the upper limit, where they noted a saturation of electron fluxes. An explanation for the saturation of electron fluxes is that local instabilities limit the electron fluxes [*Kennel and Petschek*, 1966]. *Reeves et al.* [2011] concluded that the radiation belt electron fluxes dependence on the solar wind velocity is far more complex than that observed by *Paulikas and Blake* [1979].

In this study, motivated by the recent study by *Reeves et al.* [2011], the structure selection stage of the NARMAX approach [*Billings et al.*, 1989; *Billings and Tsang*, 1989; *Wei et al.*, 2004] was utilized to indicate which combination of solar wind parameters most strongly influence the daily averaged electron fluxes at geosynchronous orbit. The advantage of the NARMAX approach is that it is able to detect a wide range of nonlinear dependancies between output and input with the use of the ERR test [*Billings et al.*, 1989; *Billings and Tsang*, 1989; *Wei et al.*, 2004].

The NARMAX methodology was initially developed for complex engineering and biological systems. The NARMAX approach uses system identification to deduce the mathematical model from recorded data sets by identifying important model terms and then estimating the unknown parameter. The aim of the NARMAX methodology is to identify physically interpretable results that can be related to physics of the underlying system. The most straight-forward application of NARMAX is to deduce, directly from input-output data, a mathematical model of a highly complex dynamical system, which cannot be deduced from first principles. There are many examples of such systems where the NARMAX approach resulted in a considerable advance; crystal growths, human brains, vision systems and stem cells.

In space physics, the NARMAX technique has been used to analyse the dynamics of plasma turbulence and to develop forecasting models for geomagnetic indices. Recently, one more application of the NARMAX approach became evident for cases when there is an absence of knowledge about the inputs of a natural dynamical system. For example, in the case of the solar wind-magnetosphere coupling, many combinations of solar wind parameters have been proposed as coupling functions. Previously, data based assessments of these coupling functions exploited the correlation function [*Newell et al.*, 2007]. However, since the correlation function is designed to study the possible causal relationships for linear systems, the application to nonlinear solar-terrestrial systems is at the least doubtful and can be misleading.

The ERR is the basis of the NARMAX model structure selection stage, which to some extent plays the same role as the correlation function but for nonlinear systems, since the ERR quantifies the causal relationship between variables. The ERR has been employed to analyse how the previously proposed coupling functions relate to the magnetic storms and the evolution of the *Dst* index [*Balikhin et al.*, 2010; *Boynton et al.*, 2011b]. This lead to the discovery of an omission in the analytical derivation of the coupling function by [*Kan and Lee*, 1979]. In the present study, the same approach was used to determine the solar wind inputs that control the fluxes of energetic electrons at the geosynchronous orbit.

This approach has already been applied for the 1.8-3.5 MeV electron fluxes in the paper by *Balikhin et al.* [2011]. The NARMAX analysis employed daily averaged solar wind parameters from the OMNI Website, to obtain the parameters that most influenced the 1.8-3.5 MeV electron fluxes. The analysis unexpectedly identified the solar wind density to be the most efficient control parameter in this energy range. When analysing the data further with the aid of scatter plots, it was found that the velocity at which saturation takes place, and the value of the flux that corresponds to the saturation, decrease with the increase of density.

The present investigation expands the NARMAX analysis to the fluxes of electrons in other energy ranges. Section 2 details the data and methodology employed for the NARMAX analysis and the results of this are described in Section 3. These results are discussed in Section 4 and confirmed with plots of the solar wind parameters and electron fluxes.

2. The Methodology and data

The NARMAX approach [*Billings et al.*, 1989; *Billings and Tsang*, 1989; *Wei et al.*, 2004], which has been developed by *Leontaritis and Billings* [1985a, b], is one of the most advanced methodologies in nonlinear system identification. It deals with complex dynamical systems that evolve under an external input influence for which their mathematical models are not yet derived from first principles. An obvious example is the terrestrial magnetosphere or the population of the radiation belts, which evolve under the influence of the solar wind. The complete set of parameters that uniquely determines the state of such systems are also often unknown. However, the measurements of some parameters can be implied to the system and it is assumed these measurements reflect the state of the system. These parameters are referred to as the outputs of the system. In the above examples, such outputs might be geomagnetic indices in the case of the magnetosphere or high energy fluxes in the case of radiation belts. Recently, *Boynton et al.* [2011a] derived a NARMAX model of the Dst index that was shown to be competitive with respect to the Dst model by *Temerin and Li* [2006] in the study by *Ji et al.* [2012]. The assumption, which forms the basis of NARMAX, is that the output at time t can be represented as a function of the previous values of inputs $u(t)$, output $y(t)$ and noise $e(t)$, as described by (1) [*Billings et al.*, 1989; *Billings and Tsang*, 1989; *Wei et al.*, 2004].

$$\begin{aligned} y(t) \; = \; & F[y(t-1), ..., y(t-n_y), \\ & u_1(t-1), ..., u_1(t-n_{u_1}), ..., \\ & u_m(t-1), ..., u_m(t-n_{u_m}), ..., \\ & e(t-1), ..., e(t-n_e)] + e(t) \end{aligned} \tag{1}$$

where $F[\cdot]$ is some nonlinear function, y, u, and e are the output, input and noise respectively, m is the number of inputs to the system and n_y, n_{u_1},..., n_{u_m}, n_e are the maximum time lags of the output, the m inputs and the noise respectively. NARMAX is based on the expansion of $F[\cdot]$ in terms of polynomials, rational functions, B-Splines, radial basis functions etc. The full NARMAX algorithm is beyond the scope of this paper but a detailed explanation can be found in *Billings et al.* [1989].

The NARMAX methodology consists of three stages. The first stage is the model structure selection, aimed to determine the most significant model terms by evaluating all the possible combinations of the past inputs and past outputs. The second stage, parameter estimation, calculates the coefficients for each of the terms identified by structure selection. The final stage is model validation.

In this study, the model structure selection stage of the NARMAX OLS-ERR algorithm, was employed to assess which solar wind control parameters are the most important for the daily variation of electron flux, for the various energy ranges at the geosynchronous orbit. The algorithm is able to determine the combination of cross-coupled solar wind parameters, in the order of their contribution to the output, by the use of the ERR. The ERR explains the contribution to the output variance by a particular selected model term. Therefore, a high ERR indicates that a term makes a significant contribution to the output variance.

The electron flux data, for energies ranging from 24.1 keV to 3.5 MeV, were obtained from the Los Alamos National Laboratory (LANL) Synchronous Orbit Particle Analyzer (SOPA) instruments and is available at ftp:/ftp.agu.org/apend/ja/2010ja015735 [*Reeves et al.*, 2011]. The daily averages from each of the geosynchronous satellites, available on any given day, were combined into a single uniform daily average. These data were published alongside the *Reeves et al.* [2011] paper as auxiliary material and contain a description of the data set preparation. The data used in this study, therefore covers the same time period as that used by *Reeves et al.* [2011], from the 22$^{\text{nd}}$ September 1989 to the 31$^{\text{st}}$ of December 2009.

SOPA data are used for the thirteen evaluated electron fluxes from 24.1 keV to 2.0 MeV. The procedure by *Cayton and Tuszewski* [2005] was used to evaluate these fluxes at fixed energies. The method involves using Monte Carlo simulations of the instrument response as a function of energy and penetrating backgrounds, to fit a relativistic bi-Maxwellian spectrum for the count rates. The obtained spectrum was then employed to evaluate the fluxes at fixed virtual energy channels. It should be noted that the 24.1 keV and 2.0 MeV evaluated energies are extrapolations of the fit and may be less reliable than the other virtual channels. The 1.8-3.5 MeV electron flux is from a channel on the Energetic Sensor for Particles (ESP). The exact methodology of the data processing is beyond the scope of this study but details can be found in the auxiliary material to the *Reeves et al.* [2011] paper.

The daily averaged solar wind data were obtained from the OMNI website for the same time period and therefore, it is the daily average as measured at the L1 point. These data included daily averages of the IMF components in GSM coordinates, B_x, B_y, and B_z, solar wind velocity V, density n and dynamic pressure p.

Out of the 7405 day period, only 7113 days are available from the SOPA instrument (the thirteen energies from 241.1 keV to 2.0 MeV) and only 7186 are available from the ESP instrument (1.8-3.5 MeV energy). The solar wind data were even more susceptible to missing data with only 6735, 6750 and 6780 points available for the density, velocity and IMF components respectively. These missing data could be filled in by the Qin-Denton solar wind model [*Qin et al.*, 2007]. However, this was not considered in the present study.

The NARMAX OLS-ERR algorithm requires equally spaced sampled data, with longer data sets yielding more reliable results. Due to the intermittent data gaps in both the electron flux data and the solar wind data, it was difficult to obtain uninterrupted data sections, of a significant length, for use in the NARMAX OLS-ERR algorithm. Therefore, it was decided to apply linear interpolation to the data gaps with ≤ 5 missing points in both electron flux and solar wind data. This was then searched for data sections with a length of over 250 days. This resulted in 8 data sets suitable for use in the NARMAX OLS-ERR algorithm, adding up to a total of 6076 days of data.

The NARMAX OLS-ERR algorithm was applied to each of the 14 energies. For each of the energies, the electron flux, for that specific energy or energy range, was employed to be the output. The inputs to the NARMAX OLS-ERR algorithm were the solar wind parameters, V, n, p, B_x, B_y and B_z. The NARMAX OLS-ERR algorithm was run for each of the 8 data sets with a maximum second order nonlinearity, so that all quadratic coupling between the solar wind parameters were searched. The top 20 terms selected, with the highest ERR, in each of these data sets were then saved along with their ERR and the number of data points in the data set, N. The ERR was then averaged for each term over the 8 data sets, taking into account the number of data points in each of the data sets. Therefore, the average ERR, $\overline{ERR}_i$, for the term i was calculated by

$$\overline{ERR}_i = \frac{\sum_{j=1}^{N_{ds}} \left(ERR_i^{(j)} N^{(j)} \right)}{\sum_{j=1}^{N_{ds}} N^{(j)}} \tag{2}$$

where N_{ds} is the number of data sets and the j indicates which data set the ERR and N belong. If a term was not selected in one of the data sets k, but was selected in at least one data set, then the $ERR_i^{(k)}$ was taken to be zero, since below the 20th term selected, the ERR was of the order of $10^{-5}\%$ in this study. The top terms were then ordered from highest to lowest average ERR (displayed as ERR in the tables). Thus, quantifying from most appropriate to least appropriate, the contribution of each model term to the evolution of the electron flux at geosynchronous orbit.

Only the top 20 model terms with the highest ERR were found for each data set. The NARMAX OLS-ERR algorithm was limited so that it only selected the top 20 terms because the sum of ERR for all terms after the first 20 terms was negligible in comparison with ERR of the most important terms. The algorithm was set to search through 5 time lags of the inputs. Since the data are averaged over a day, it is possible for the averaged solar wind parameter for one day to causally affect the average energy fluxes for that same day. Therefore, the time lags corresponded to the current day (time lag equals to zero) and four previous days (time lags from 1 to 4). For this study, the aim was just to identify what solar wind parameters influenced the energetic electron fluxes in the radiation belt. Therefore, the past values of the output were not included in the search.

3. Results of the ERR analysis

Tables 1, 2, 3 and 4 display the results of the NARMAX algorithm for all electron energies considered in this study. The top 5 terms are shown in the order of the ERR and the number of data sets in which the term was selected are also shown. Therefore, out of the possible 8 data subintervals, the number of times selected is in how many subintervals the NARMAX selected this parameter. The tables show that for all but two of the energies the velocity explains most of the electron flux variance, as observed by *Paulikas and Blake* [1979] and more recently by *Reeves et al.* [2011]. For energies from 24.1 keV to 925 keV, the velocity accounts for over 95% of the explained dependent variable variance or ERR. In addition, another $1 - 3\%$ of the ERR results from the quadratic velocity terms, V^2.

For the electron flux evaluated at 2.0 MeV and in the energy range 1.8-3.5 MeV, the density explains the majority of the ERR. For 1.8-3.5 MeV electron flux, the previous day's density accounts for over 50% of the ERR and the fact that the term is selected in each of the data sets, suggests that this is not an erroneous result. The density squared for the previous day explains the second highest amount of the variance. However, the time lags of the velocity squared still play a significant role in the dynamics of 1.8-3.5 MeV electrons, since the two velocity squared terms explain over 10% of the ERR. The coupling between density and velocity also appear to play a minor role in both the electron flux evaluated at 2.0 MeV and in the energy range 1.8-3.5 MeV, with pV (nV^3) and np (n^2V^2) accounting for about 3% of the ERR.

The north-south IMF component, B_z, which is employed as an input in one of the most well known radiation belt forecasting models by *Li et al.* [2005] was only found to have a very negligible influence on the electron fluxes. The B_z parameter never accounts for more than a tenth of a percent for all the energies. This was unforeseen since B_z is the parameter that controls the initiation of magnetospheric disturbances such as storms and substorms. Such an independence can be explained by the shorter time scales of the B_z dynamics. While the electron flux evolution time scale is of the order of days, the typical temporal variation of B_z is of the order of hours. The daily average values of B_z may hide the dynamics that occur on a shorter time scale of a few hours. To find the possible effects of these shorter time scale variations in B_z on high energy electrons, two extra parameters were included in additional runs. The first one, τ_{B_s}, is the daily integral duration of the negative B_z periods, i.e. the cumulative time that the IMF had a southward orientation, B_s, within each day. The second one is daily integral value of B_s, $I_{B_s} = \int B_s dt$. However, neither of these two parameters had prominent ERR values and therefore they are not crucial in the control of high energy fluxes.

It is obvious from Tables 1, 2 and 3 that the time delays between the solar wind velocity, as a control parameter, and fluxes of energetic electrons are not constant but depend upon the energy. In the case of the five lowest energies, from 24.1 keV to 90.0 keV, the current day's velocity accounts for most of the ERR. For the electron flux evaluated at 127.5 keV, the previous day's velocity provides a significant contribution to the ERR, however, this contribution is still inferior to that of the current day's velocity. For the next energy up, 172.5 keV, the contribution of the previous day's solar wind velocity becomes dominant. At the higher energy of 270 keV, it is still the case and in comparison to lower energy of 172.5keV, the ERR resulting from current day's velocity is negligible. The fluxes evaluated at 407 keV and 625 keV display an increasing significance of the velocity from two days in the past. For the two next energies of 925 keV and 1.3 MeV, the solar wind velocity from two days in the past dominates the ERR.

The results shown in Tables 1, 2, 3 and 4 were constrained to a second order nonlinearity with 5 time lags for simplicity. To determine if the initial constraints were valid, the NARMAX analysis was run again with a fourth order nonlinearity and 10 time lags (the current day at time t and the time lags for the previous 9 days). However, the most appropriate terms did not change from Tables 1, 2, 3 and 4. Therefore, for these energies, the initial constraints of a second order nonlinearity and 5 time lags were suitable. It must be noted that the numbers for the 1.8-3.5 MeV energy range in Table 4 differ from those presented by *Balikhin et al.* [2011] but are still close to these values. This is because a different averaging procedure was employed. The duration of each of the data sets was not taken into account for the averaging procedure used by *Balikhin et al.* [2011], but has been taken into account in the present study.

4. Discussion

It is evident from Tables 1, 2, 3 and 4 that for lower energy electrons the solar wind velocity is indeed the most important parameter that determines the energetic electron fluxes at geosynchronous orbit. As it was noted above, the fluxes of the lower energies (up to 90 keV) are controlled by the value of the current day's solar wind velocity and the effects of the previous values of the velocity are negligible. However, for the 127.5 keV electron fluxes, the influence of the solar wind velocity for the previous day become significant, around 22% (Table 2). For the next energy, of 172.5 keV, the value of the previous day's velocity becomes dominant (65%), while the current day's velocity still contributes to about of 32.5% of variance, if both terms $V(t)$ and $V^2(t)$ are taken into account. Starting from 270 keV the contribution of the current day's velocity accounts for less than 0.02% of variance. Therefore, the effects of the present day's velocity can be neglected. For even higher energy electrons, the effects of the solar wind velocity registered 2, 3 or 4 days in the past appear.

This dependence between the time delay and the energy has been detected before [*Li*, 2004; *Li et al.*, 2005]. In general, such a relationship is in complete accordance with the local quasilinear diffusion model, in which the acceleration processes acting on the same seed population, lead to a build up of electron fluxes with higher and higher energies. *Li et al.* [2005] argued that this can be explained by radial diffusion and suggested that it takes longer for higher energy electrons to reach geosynchronous orbit. The diffusion type of acceleration is a relatively slow process, where the energy change should be proportional to the square root of time. The ERR results can aid in quantifying the dependence between the time delay, τ, and the energy of the electron fluxes, E. The effective time delay τ_k, for a particular energy k, can be estimated as

$$\tau_k = \frac{S_{1k} + 2S_{2k} + 3S_{3k} + 4S_{4k}}{S_{0k} + S_{1k} + S_{2k} + S_{3k} + S_{4k}} \tag{3}$$

where S_{ik} is the sum of ERR values corresponding to the energy range k for all the terms of the solar wind velocity i days in the past. The resulting energy vs. effective time delay plot is displayed in Figure 1. All of the points, except the one that corresponds to the lowest energy value (127.5 keV), almost perfectly fit a straight line on this log-log scale, with a gradient of about 1.5. Fitting a linear gradient for a line that includes the lowest energy, leads to a smaller gradient of around 1.05. Both of these numbers indicate that the increase in energy takes place much faster than that expected from a diffusion type process, which takes place in the energy space if the initial seed population possesses very low energies. Otherwise the increase of the fluxes in higher energy will reflect not only the speed of energization but also properties of the initial seed distribution.

The NARMAX algorithm is a very complex mathematical tool. Therefore, it is beneficial for readers in scientific fields who are not accustomed to the complex type of mathematics used in systems science, if the results of the NARMAX analysis can be illustrated by simpler means. Hence, it is better to verify the ERR deduced dependence, between the effective time delay and the energy, on a particular example.

Figure 2 displays an event in the solar wind velocity (black) and the resulting effect on the 24.1 keV (blue), 270 keV (red) and 925 keV (green) electron fluxes. The figure shows an increase in velocity on the 26th February 2004 (left dashed line), which is followed on the same day with an increase in the 24.1 keV electron flux. The next day (middle dashed line), an increase in the 270 keV electron flux can be observed. Finally (right dashed line), there is an increase in the 925 keV electron flux, two days after the initial increase in velocity. The change of the time delay with energy observed in Figure 2 agrees with the ERR results.

Since the NARMAX analysis provides a quantitative assessment of this dependence, the results can be used to evaluate the efficiency of both radial diffusion and energy diffusion due to the interactions with waves. It is well known that in the case of diffusion equations with constant coefficients, characteristic changes should be proportional to the square root of time. However, the energy diffusion equations are more complex *Horne et al.* [2005]:

$$\frac{\partial F}{\partial t} = \frac{\partial}{\partial E}\left[A(E)D_{EE}\frac{\partial}{\partial E}\left[\frac{F}{A(E)}\right]\right] - \frac{F}{\tau_L} \tag{4}$$

Where A is defined as:

$$A = (E+E_0)(E+2E_0)^{\frac{1}{2}}E^{\frac{1}{2}} \tag{5}$$

F is a distribution function, E is the kinetic energy, D_{EE} is the bounce-averaged energy diffusion coefficient, τ_L is the effective timescale for losses to the atmosphere and E_0 is the rest energy of the electron.

The distribution function $F(E, \alpha_{eq})$, which depends upon energy E and the equatorial pitch angle α_{eq}, is related to the fluxes $J(E, \alpha_{eq})$ [*Horne et al.*, 2005]

$$F(E, \alpha_{eq}) = \frac{E + E_0}{c(E + 2E_0)^{\frac{1}{2}} E^{\frac{1}{2}}} J(E, \alpha_{eq}) \tag{6}$$

Balikhin et al. [2012] studied the upper limit on the time dependence of increases in the flux using the energy diffusion equation above. They concluded that in the 3 cases; (1) $E \ll E_0$; (2) $E \approx E_0$; and (3) $E \gg E_0$, the characteristic time scale is very close to the expected form of a simple diffusion equation, i.e., proportional to the square root of time. In observing such a relationship, it would take the 900 keV electron fluxes 25 times longer to build than the 175 keV electron fluxes. The dependence displayed in Figure 1 is much faster. This is the argument in favour of radial diffusion being significantly more efficient, at geosynchronous orbit, in comparison to the effects of local wave-particle interactions.

However, it must be noted that the square root dependence upon time, deduced analytically by *Balikhin et al.* [2012], used a number of simplifications. The loss term, τ_L, describes the effect of particle precipitation in the loss cone. This effect can only slow down acceleration and therefore neglecting this term will only reduce the time required for acceleration. The time dependence was deduced separately for the 3 energy cases to simplify the dependence of A upon E. Also, it was assumed that the diffusion coefficient D_{EE}, is independent of energy. Although general considerations do support these assumptions, numerical simulations are the best way to verify them.

While the dependence of the energy upon the time delay corresponds to the current models of acceleration, the appearance of the solar wind density as the main controlling factor for the energy channels 2.0 MeV and 1.8-3.5 MeV, cannot be deduced from the current models of acceleration. Some models relate the dynamic pressure to ULF waves, but all the terms that involve pressure have a very low ERR. The importance of the solar wind density, for the 1.8-3.5 MeV electron fluxes, have already been identified in *Balikhin et al.* [2011] by the same ERR based technique. It was argued that under a constant density, the electron fluxes in this energy range initially increase with velocity but at some point reach the saturation. *Balikhin et al.* [2011] stated that both the level of the flux, which corresponds to the saturation, and the velocity that the saturation takes place, decrease with the increase of density. They also included scatter plots, which showed that the top fluxes in this energy range correspond to low solar wind density on the previous day.

Figure 3 represents a velocity vs. density scatter plot similar to *Balikhin et al.* [2011], where each point corresponds to a particular day in the period from the 22nd September 1989 to the 31st of December 2009. The red points, in panels (a) and (b), illustrate the days with the highest 5% of the 24.1 keV electron flux (above $10^{5.6}(\mathrm{cm}^3 \cdot \mathrm{s} \cdot \mathrm{sr} \cdot \mathrm{keV})^{-1}$), while the red points in panel (c) correspond to the days with the highest 5% of the 1.8-3.5 MeV electron flux (above $10^{0.76}(\mathrm{cm}^3 \cdot \mathrm{s} \cdot \mathrm{sr} \cdot \mathrm{keV})^{-1}$). The blue in all the panels is used to show all of the other days with lower fluxes.

Figure 3(c) displays the solar wind velocity from two days in the past against the previous day's solar wind density. These lags were selected because they correspond to the velocity and density terms with the highest ERR for the 1.8-3.5 MeV electron flux.

The figure confirms the conclusion of *Balikhin et al.* [2011], which was that the majority of high 1.8-3.5MeV fluxes occur when low solar wind densities are observed on the previous day. Figures 3(a) and 3(b) represent similar plots but for an energy of 24.1 keV. Figure 3(a) shows the current day's solar wind velocity vs. the current day's solar wind density, again, selecting the lags that correspond to the velocity and density terms with the highest ERR for the 24.1 keV electron flux. The figure shows that high fluxes occur at all densities and velocities, implying that there is no relationship. Figure 3(b) displays the current day's solar wind velocity vs. the previous day's solar wind density. This figure was included to illustrate that there is also no relationship when the previous day's density is employed for the 24.1 keV electron flux. It is obvious in Figure 3(c) that the high fluxes occur when there is low density, yet this relationship is absent in Figures 3(a) and 3(b).

However, in Figure 3(c), velocities above 600 kms^{-1} only occur when the density is low. Figure 4(a) shows, for each velocity bin of 25 kms^{-1}, the probability of each density bin, of 0.5 cm^{-3}, corresponding to the highest 5% of the 1.8-3.5 MeV electron flux. This probability is then normalised across each of the velocity bins, to highlight the density with the maximum probability. Figure 4(b) displays the probability of a density occurring for each velocity, employing the same bin dimensions and normalization across the velocity used to calculate Figure 4(a). Panel (a) illustrates that low solar wind densities on the previous day, have a higher probability of producing a high flux at all velocities. If this is just because high velocities only occur when the density is low, panel (b) should have the same pattern as panel (a). However, for velocities lower than 600 kms^{-1}, panel (b) displays a more spread distribution, which peaks at a higher density, compared to panel (a). For the 400-425 kms^{-1} velocity bin, the probability of a density occurring, peaks at the 5-5.5 cm^{-3} density bin, while the probability of a highest 5% 1.8-3.5 MeV electron flux occurring peaks at the 4-4.5 cm^{-3}.

This is implicit confirmation of the ERR results presented in Table 4. It must be noted that the effects of the solar wind density are evident in the ERR results, for energies starting from 925 keV, where the solar wind density is the is the second most important factor after $V(t-2)$ but with a very low ERR value. For the next energy range of 1.3 MeV, the density, as a factor of nV, appears in the second and third most important controlling terms of the electron flux. As it was noted, the density is the main controlling factor for the two highest energy channels.

Figure 5 displays the solar wind parameters and three energies of the electron flux for the period between 7th November 2000 and 23th November 2000. In panel (a), an increase in velocity is shown, peaking at 900 km/s, which results in an increase in electron flux for the three energies shown in panels (d), (e) and (f) and panel (g) displays the magnetopause position along the Earth-Sun line according the model by *Shue et al.* [1997] in grey, with the black dashed line indicating geosynchronous orbit. For the highest energy range in panel (d), the 1.8-3.5 MeV electron flux then remains at the same level while the velocity decreases. A loss of electrons is then observed on 18th November 2000. This occurs while the velocity is low, approximately 300 kms^{-1}, as such the increase in solar wind density to 18 cm^{-3} only results in a relatively small increase of the ram pressure of about 4 nPa. Compared to the similar density on the 10th November 2000, when the solar wind is above 900 kms^{-1}, the increase in ram pressure is much larger, above 30 nPa. The relative change in density on the 18th November 2000 is quite high compared to other changes in density but, due to the low velocity, the change in pressure is relatively low compared to the change in pressure on 10th November 2000.

For the electron fluxes with energies below 925 keV, where the ERR results showed that there was no dependence with density, the fluxes start to decrease immediately after it has peaked and does not plateau like the higher energies as shown in panel (d). Panel (e) shows the 635 keV flux starts to decrease with a slight slope after it peaks and, thus, has already decreased before the density increase. While in panel (f) the 270 keV flux displays an even greater decay of electrons after it peaks, depicting a more obvious relationship with velocity. These, and other energy ranges that are not shown in Figure 5, seem to imply that the decrease of solar wind velocity leads to the depletion of electron fluxes. However, the rate of this depletion depends upon the energy range, decreasing with the increase of energy. For high energies such as 1.8-3.5 MeV, the rate of depletion is so small that the decrease of fluxes is not evident for this energy. Therefore, for the higher energy electrons, the fluxes increase with an increase in solar wind velocity but then plateaus rather than decreases with time. The fluxes in the range 1.8-3.5 MeV remain roughly constant until there is a relatively high increase in solar wind density, which results in a significant reduction in the flux of 1.8-3.5 MeV electrons.

Panel (g) of Figure 5 shows that on the 18th November 2000 the magnetopause does not drop below 9 R_E. However, on the 10th November 2000, when another decrease in flux is observed, the magnetopause moves within geosynchronous orbit and thus the loss is most likely due to magnetopause shadowing [*Onsager et al.*, 2007; *Ohtani et al.*, 2009; *Matsumura et al.*, 2011]. The example that is shown in Figure 5 provides evidence that, at least in some cases, the reduction in electron flux is associated with density enhancement, since the corresponding pressure change is small. This effect can be attributed to waves that cause losses [*Loto'aniu et al.*, 2010].

One possible explanation for the density dependence at high energies is that the various ULF fluctuations at the boundaries of magnetosphere could be in resonance with electrons of this particular energy. For example, it is well known that the threshold of the Kelvin-Helmholtz instability is [*Chandrasekhar*, 1961; *Otto and Fairfield*, 2000]:

$$[\mathbf{k}\cdot(\mathbf{V_1}-\mathbf{V_2})] > \frac{n_1+n_2}{4\pi m_0 n_1 n_2}[(\mathbf{k}\cdot\mathbf{B_1})^2+(\mathbf{k}\cdot\mathbf{B_2})^2], \tag{7}$$

where m_0 is the ion mass, B is the magnetic field and the indices correspond to the two regions across the shear layer. In the case of a parallel propagation with the same Alfven velocity (V_A) across the flow shear layer, the threshold becomes equal to $2V_A$. While the threshold does indeed exhibit a density dependence, it is the opposite from what is needed to explain the ERR results, since the threshold increases with the decrease in density. The growth rate, γ, of a classical Kelvin-Helmholtz instability has been calculated many times [*Mikhailovskii and Klimenko*, 1980]:

$$\gamma = \frac{k_{\parallel}V_A}{2}\left[\left(\frac{V^2}{V_A^2}\right)-4\right]^{\frac{1}{2}} \tag{8}$$

Again, the growth rate does not increase with the decrease in density. The other possibility is the saturation of the Kelvin-Helmholtz instability. *Golikov et al.* [1980] have shown that unless:

$$\left(\frac{n_i}{n_e}\right)^{\frac{1}{2}} < \frac{B_e}{B_i} \tag{9}$$

the instability is stabilised by the sausage mode. Here, the indices i and e notate the parameters inside and external to the layer of flow along the magnetopause in which the instability develops. The stabilization criteria of the Kelvin-Helmholtz instability at the magnetopause should be recalculated in the conditions that are more realistic than those used by *Golikov et al.* [1980]. In general, the decrease in solar wind density should lead to the decrease of the magnetosheath density. The density downstream of the collisionless shock is related to the upstream density by a factor that decreases with the decrease in Mach number. The decrease of the solar wind density leads to the decrease of Alfven Mach number, (providing that other parameters are constant) and therefore, the decrease of the magnetosheath density. A realistic estimate must include a dependence of n_i, determined by the magnetosheath density.

It is worth noting the Kelvin-Helmholtz is only one of the very many possible instabilities that can affect radial diffusion or be related to other models of electron acceleration. However, a comprehensive survey of the density effects on these instabilities is beyond the scope of the present paper.

The other interesting result of ERR analysis is the weak statistical dependence of high energy electron enhancements upon the direction of B_z. This result disagrees with the case study by *Blake et al.* [1997], where they presented a 160 day interval, during which three significant increases in the solar wind speed of 5-10 days duration were observed. The increase of the high energy fluxes were only registered for two of these events, both of which had a substantial interval of southward IMF. During the third event, which was not accompanied by the increase of high energy electron fluxes, the IMF was only northward. *Blake et al.* [1997] concluded that the southward turning of the IMF is an important factor for the evolution of the high energy electron population. *Li et al.* [2011] suggested that high speed solar wind is almost always associated with the enhancement of high energy electrons because it almost always has some southward component of IMF.

However, *Li et al.* [2011] implicitly suggests that the Bz direction is the primary factor and the high speed streams trigger the increase of high energy fluxes because they are usually accompanied by periods of southward IMF. Such an interpretation contradicts both the ERR results presented here and many observations when the southward IMF did not lead to the increase of high energy fluxes. For example, *Reeves* [1998] found that about half of strong storms do not result in the increase of relativistic electron fluxes, which invalidates the *Li et al.* [2011] suggestion that the IMF direction is more important than other solar wind parameters, including the velocity. This independence can be explained by the shorter time scales of the B_z dynamics. The time scale of the electron flux is of the order of days, while the changing of the B_z orientation is of the order of hours. The daily averaging of B_z will mean that the shorter time scale dynamics will be lost. However, when additional runs of the ERR analysis were performed using inputs, which could account for the short time scale variations of B_z, the velocity still came out on top.

Miyoshi and Kataoka [2008a, b] performed a statistical study using a superposed epoch analysis on how stream interaction region (SIR) events effect the relativistic electron fluxes. From the Spring to and Fall away (STFA) rule, they separated the SIR events into north and south IMF configurations and found that acceleration of the electrons was larger when the IMF was south. After this, using the southward IMF SIRs, they then separated these events into high speed (>500 kms^{-1}) and low speed (<500 kms^{-1}) and showed that the slow speed SIR events have a smaller increase. They conclude by stating that both the southward IMF and solar wind velocity are important for the enhancements of the electron flux and that and the largest enhancements of the electron flux occur when the both the velocity is high and the IMF is southward. Therefore, solar wind speed by itself is not sufficient for the large electron flux increase but a southward orientated IMF is also needed. *McPherron et al.* [2009] performed a similar statistical study on SIR events to determine whether the Russell McPherron polarity effect [*Russell and McPherron*, 1973] had any influence on electron fluxes. Again, by selecting the SIR events based on the STFA rule, they performed a superposed epoch analysis. They concluded that the Russell McPherron effect has an significant role in the enhancement of electron fluxes and thus the southward component of the IMF is important.

These studies, which found the southward IMF to be an important factor in the large enhancements of the electron flux, do not contradict the ERR analysis. However, to reconcile the results of the ERR analysis presented here and the importance of the southward orientation of B_z in some previous case studies [*Blake et al.*, 1997; *Lyons et al.*, 2005] and statistical studies [*Miyoshi and Kataoka*, 2008a, b; *McPherron et al.*, 2009] the question *How can it be that a southward B_z is important for initiating the chain of physical processes that lead to the flux increase but, statistically, according to the ERR analysis, does not effect the evolution of daily fluxes?* should be answered. One of the possible answers can be the following: (1) The turning of the B_z component southward is not enough for the enhancement of the electron fluxes. (2) Something else (for example high solar wind velocity like in a SIR) is required to trigger the flux increase. (3) This ‘something else’ is almost always accompanied by B_z turning southward. (4) However, the turning of B_z southward often takes place without this ‘something else’. For example, in the case of a low speed solar wind flow for several days, there will almost certainly be periods of southward IMF, however, no flux increase will occur because a high solar wind flow is also required. While in the case of a high velocity solar wind event, taking place over several days, there is a very high probability that there will be periods of time when the IMF is southward. Therefore, over the 20 year period studied, statistically, the solar wind velocity will appear to have the most influence on the fluxes. In the former case of low solar wind velocity and a southward IMF, storm/substorm activity will be triggered but an increase of relativistic electron fluxes at geosynchronous orbit will not take place. This possible explanation has implicit support from previous studies such as *Reeves* [1998] and *Kataoka and Miyoshi* [2006]. In the latter study, it was shown that in spite of the southward orientation of B_z leading to storm/substorm activity in 49 of CME triggered events, only 43% of them resulted in the increase of the high energy electron fluxes in the outer radiation belt. At the same time, *Kataoka and Miyoshi* [2006] have reported that flux increases were observed for 83% of SIR induced events.

The reason the ERR analysis results differs from the superposed epoch analysis of *Miyoshi and Kataoka* [2008a, b]; *McPherron et al.* [2009] in regard to the importance of the southward IMF is most likely due to the intervals chosen; the ERR analysis was performed on all the available data for the 20 year period, while the superposed epoch analysis studied many SIRs interfaces. As such, a study focused solely on the SIR events, using higher resolution data, will reveal more detail of the effects on the electron fluxes associated with an SIR but miss out other dynamics. Therefore, since ERR analysis accounted for periods where there were no SIR events, where the turning of the IMF southward on its own would not lead to an enhancement of the flux, the IMF would appear to have less of an effect.

Summarizing, the ERR results presented here do not contradict the main result of *Miyoshi and Kataoka* [2008a, b]; *McPherron et al.* [2009], which state that the southward

IMF, as well as the solar wind speed, controls the flux enhancement of the outer radiation belt in the SIR events. The only difference is based on the fact that the probability for the occurrence of high speed solar wind and the probability for the occurrence of a southward IMF differ a lot. Both factors are required, however, many intervals of a southward IMF are observed without a high speed solar wind stream. On the other hand, at the leading edge of the high solar wind stream, significant variations of the IMF resulting in a southward orientation are very often observed. Therefore, while both factors are required, whenever the high speed solar wind stream is observed, there is a very high probability of intervals with a southward IMF. However, if a southward IMF intervals is observed, it does not warranty the high chance of a high speed solar wind stream. Therefore, over the entire 20 year period studied, statistically, the solar wind velocity will have the most influence on the electron flux at geosynchronous orbit, since the periods where the southward IMF does play a role (the large increase in flux due to an SIR event), only occur in a small percentage of the 20 years studied.

5. Conclusions

This study has confirmed that the solar wind velocity is indeed the main control parameter for the electron fluxes with energies below 1 MeV, which was originally observed by *Paulikas and Blake* [1979].

The results of the NARMAX analysis show a dependence between the time delay of the velocity and the energy of the electron flux. Generally, such an increase is in accordance with both the local wave-particle interaction model and the radial diffusion model in which it takes longer for higher energies to reach geostationary orbit. However, this increase occurs much faster than would be expected from a simple quasilinear diffusion model due to the interaction with local waves, providing that the seed population possesses very low energies.

This study validates the results by *Balikhin et al.* [2011], which show that the solar wind density becomes the most influential control parameter at 1.8 MeV electron fluxes. The ERR results in this study depict an increasing dependence on density above energies of 925keV. In addition to the ERR results, the scatter plots in Figure 3 show that for low energies, high fluxes appear at all densities, implying that there is no relationship between low energy electron fluxes and the solar wind density. However, for the high energy electrons, the high fluxes only occur when the density is low. This dependence upon density can be explained by the properties of instabilities related to ULF oscillations at the boundaries of the magnetosphere.

The ERR analysis has shown that statistically B_z does not affect the evolution of the daily averaged electron population at geosynchronous orbit. An explanation for this is that when high speed solar wind flow is observed, which leads to an increase in electron fluxes, it will almost always be accompanied by periods of time when the IMF is southward. However, the southward turning of the IMF occurs much more often than the high speed solar wind flows. As such, when the southward IMF occurs with a low speed solar wind flow and no electron flux increase is observed, it implies that statistically the IMF turning southward is not as important as an increase in solar wind velocity.

Acknowledgments. The authors would like to acknowledge the financial support from EPSRC, STFC and ERC. RJB and MAB are grateful for support from ISSI (Bern). The Authors would also like to thank the OMNIWeb service for providing the solar wind data and the group responsible for maintaining the in flight operations and processing the data archives for the SOPA and ESP instruments.

References

Albert, J. M., Evaluation of quasi-linear diffusion coefficients for emic waves in a multi-species plasma, *J. Geophys. Res.*, *108*(A6), 1249, 2003.

Albert, J. M., Evaluation of quasi-linear diffusion coefficients for whistler mode waves in a plasma with arbitrary density ratio, *J. Geophys. Res.*, *110*(A3), A03,218, 2005.

Baker, D. N., P. R. Higbie, R. D. Belian, and J. Hones, E. W., Do jovian electrons influence the terrestrial outer radiation zone?, *Geophys. Res. Lett.*, *6*(6), 531–534, 1979.

Baker, D. N., R. L. McPherron, T. E. Cayton, and R. W. Klebesadel, Linear prediction filter analysis of relativistic electron properties at 6.6 re, *J. Geophys. Res.*, *95*(A9), 15,133–15,140, 1990.

Balikhin, M. A., R. J. Boynton, S. A. Billings, M. Gedalin, N. Ganushkina, D. Coca, and H. Wei, Data based quest for solar wind-magnetosphere coupling function, *Geophys. Res. Lett.*, *37*(24), L24,107, 2010.

Balikhin, M. A., R. J. Boynton, S. N. Walker, J. E. Borovsky, S. A. Billings, and H. L. Wei, Using the narmax approach to model the evolution of energetic electrons fluxes at geostationary orbit, *Geophys. Res. Lett.*, *38*(18), L18,105, 2011.

Balikhin, M. A., M. Gedalin, G. D. Reeves, R. J. Boynton, and S. A. Billings, Time scaling of the electron flux increase at geo: The local energy diffusion model vs observations, *J. Geophys. Res.*, *117*(A10), A10,208–, 2012.

Billings, S., S. Chen, and M. Korenberg, Identification of mimo non-linear systems using a forward-regression orthogonal estimator, *Int. J. Control*, *49(6)*, 2157–2189, 1989.

Billings, S. A., and K. M. Tsang, Spectral analysis for nonlinear systems, part i: Parametric non-linear spectral analysis, *Mech. Syst. Signal Proc.*, *3*, 319–339, 1989.

Blake, J. B., W. A. Kolasinski, R. W. Fillius, and E. G. Mullen, Injection of electrons and protons with energies of tens of mev into l¡3 on 24 march 1991, *Geophys. Res. Lett.*, *19*(8), 821–824, 1992.

Blake, J. B., D. N. Baker, N. Turner, K. W. Ogilvie, and R. P. Lepping, Correlation of changes in the outer-zone relativistic-electron population with upstream solar wind and magnetic field measurements, *Geophys. Res. Lett.*, *24*(8), 927–929, 1997.

Boscher, D., S. Bourdarie, R. Thorne, and B. Abel, Influence of the wave characteristics on the electron radiation belt distribution, *Advances in Space Research*, *26*(1), 163–166, 2000.

Boynton, R. J., M. A. Balikhin, S. A. Billings, A. S. Sharma, and O. A. Amariutei, Data derived narmax dst model, *Annales Geophysicae*, *29*(6), 965–971, doi:10.5194/angeo-29-965-2011, 2011a.

Boynton, R. J., M. A. Balikhin, S. A. Billings, H. L. Wei, and N. Ganushkina, Using the narmax ols-err algorithm to obtain the most influential coupling functions that affect the evolution of the magnetosphere, *J. Geophys. Res.*, *116*(A5), A05,218, 2011b.

Cayton, T. E., and M. Tuszewski, Improved electron fluxes from the synchronous orbit particle analyzer, *Space Weather*, *3*(11), S11B05–, 2005.

Chandrasekhar, S., *Hydrodynamic and Hydromagnetic Stability*, Oxford Univ. Press, New York, 1961.

Elkington, S. R., M. K. Hudson, and A. A. Chan, Acceleration of relativistic electrons via drift-resonant interaction with toroidal-mode pc-5 ulf oscillations, *Geophys. Res. Lett.*, *26*(21), 3273–3276, 1999.

Falthammar, C.-G., *Radial Diffusion by Violation of the Third Adiabatic Invariant*, 157 pp., Reinhold, New York, 1968.

Friedel, R., G. Reeves, and T. Obara, Relativistic electron dynamics in the inner magnetosphere - a review, *Journal of Atmospheric and Solar-Terrestrial Physics*, *64*(2), 265–282, 2002.

Fujimoto, M., and A. Nishida, Energization and anisotropization of energetic electrons in the earth's radiation belt by the recirculation process, *J. Geophys. Res.*, *95*(A4), 4265–4270, 1990.

Golikov, Y., T. Plyasova-Bakounina, V. Troitskaya, A. Chernikov, V. Pustovalov, and P. Hedgecock, Where do solar wind-controlled micropulsations originate?, *Planetary and Space Science*, *28*(5), 535–543, 1980.

Horne, R. B., R. M. Thorne, S. A. Glauert, J. M. Albert, N. P. Meredith, and R. R. Anderson, Timescale for radiation belt electron acceleration by whistler mode chorus waves, *J. Geophys. Res.*, *110*(A3), A03,225, 2005.

Hudson, M., S. Elkington, J. Lyon, and C. Goodrich, Increase in relativistic electron flux in the inner magnetosphere: Ulf wave mode structure, *Advances in Space Research*, *25*(12), 2327–2337, 2000.

Hudson, M. K., S. R. Elkington, J. G. Lyon, C. C. Goodrich, and T. J. Rosenberg, Simulation of radiation belt dynamics driven by solar wind variations, in *Geophys. Monogr. Ser.*, vol. 109, pp. 171–182, AGU, Washington, DC, 1999.

Hudson, M. K., S. R. Elkington, J. G. Lyon, M. Wiltberger, and M. Lessard, Radiation belt electron acceleration by ulf wave drift resonance: Simulation of 1997 and 1998 storms, in *Space Weather*, pp. 289–296, Geophys. Monogr., 2001.

Ji, E.-Y., Y.-J. Moon, N. Gopalswamy, and D.-H. Lee, Comparison of dst forecast models for intense geomagnetic storms, *J. Geophys. Res.*, *117*(A3), A03,209–, 2012.

Kan, J. R., and L. C. Lee, Energy coupling function and solar wind-magnetosphere dynamo, *Geophys. Res. Lett.*, *6*, 577–580, 1979.

Kataoka, R., and Y. Miyoshi, Flux enhancement of radiation belt electrons during geomagnetic storms driven by coronal mass ejections and corotating interaction regions, *Space Weather*, *4*(9), S09,004–, 2006.

Kennel, C., and H. Petschek, Limit on stably trapped particle fluxes, *J. Geophys. Res.*, *71(1)*, 1–28, 1966.

Leontaritis, I. J., and S. A. Billings, Input-output parametric models for non-linear systems part i: Deterministic non-linear systems., *Int. J. Control*, *41 (2)*, 303–328, 1985a.

Leontaritis, I. J., and S. A. Billings, Input-output parametric models for non-linear systems part ii: Stochastic nonlinear systems, *Int. J. Control*, *41 (2)*, 329–344, 1985b.

Li, X., Variations of 0.7-6.0 mev electrons at geosynchronous orbit as a function of solar wind, *Space Weather*, *2*(3), S03,006, 2004.

Li, X., M. Temerin, D. N. Baker, and G. D. Reeves, Behavior of mev electrons at geosynchronous orbit during last two solar cycles, *J. Geophys. Res.*, *116*(A11), A11,207–, 2011.

Li, X. L., M. Temerin, D. N. Baker, G. D. Reeves, and D. Larson, Quantitative prediction of radiation belt electrons at geostationary orbit based on solar wind measurements, *Geophys. Res. Lett.*, *28*(9), 1887–1890, 2001.

Li, X. L., D. N. Baker, M. Temerin, G. Reeves, R. Friedel, and C. Shen, Energetic electrons, 50 kev to 6 mev, at geosynchronous orbit: Their responses to solar wind variations, *Space Weather*, *3*(4), S04,001, 2005.

Liu, W. W., G. Rostoker, and D. N. Baker, Internal acceleration of relativistic electrons by large-amplitude ulf pulsations, *J. Geophys. Res.*, *104*(A8), 17,391–17,407, 1999.

Loto'aniu, T. M., H. J. Singer, C. L. Waters, V. Angelopoulos, I. R. Mann, S. R. Elkington, and J. W. Bonnell, Relativistic electron loss due to ultralow frequency waves and enhanced outward radial diffusion, *J. Geophys. Res.*, *115*(A12), A12,245–, 2010.

Lyons, L. R., D.-Y. Lee, R. M. Thorne, R. B. Horne, and A. J. Smith, Solar wind-magnetosphere coupling leading to relativistic electron energization during high-speed streams, *J. Geophys. Res.*, *110*(A11), A11,202–, 2005.

Matsumura, C., Y. Miyoshi, K. Seki, S. Saito, V. Angelopoulos, and J. Koller, Outer radiation belt boundary location relative to the magnetopause: Implications for magnetopause shadowing, *J. Geophys. Res.*, *116*(A6), A06,212–, 2011.

McPherron, R., D. Baker, and N. Crooker, Role of the russell-mcpherron effect in the acceleration of relativistic electrons, *Journal of Atmospheric and Solar-Terrestrial Physics*, *71*(1011), 1032–1044, 2009.

Mikhailovskii, A. B., and V. A. Klimenko, The microinstabilities of a high β plasma flow with a non-uniform velocity profile, *Journal of Plasma Physics*, *24*(03), 385–407, 1980.

Miyoshi, Y., and R. Kataoka, Flux enhancement of the outer radiation belt electrons after the arrival of stream interaction regions, *J. Geophys. Res.*, *113*(A3), A03S09–, 2008a.

Miyoshi, Y., and R. Kataoka, Probabilistic space weather forecast of the relativistic electron flux enhancement at geosynchronous orbit, *Journal of Atmospheric and Solar-Terrestrial Physics*, *70*(24), 475–481, 2008b.

Newell, P. T., T. Sotirelis, K. Liou, C. I. Meng, and F. J. Rich, A nearly universal solar wind-magnetosphere coupling function inferred from 10 magnetospheric state variables, *J. Geophys. Res.*, *112*, A01,206, 2007.

O'Brien, T. P., K. R. Lorentzen, I. R. Mann, N. P. Meredith, J. B. Blake, J. F. Fennell, M. D. Looper, D. K. Milling, and R. R. Anderson, Energization of relativistic electrons in the presence of ulf power and mev microbursts: Evidence for dual ulf and vlf acceleration, *J. Geophys. Res.*, *108*(A8), 1329, 2003.

Ohtani, S., Y. Miyoshi, H. J. Singer, and J. M. Weygand, On the loss of relativistic electrons at geosynchronous altitude: Its dependence on magnetic configurations and external conditions, *J. Geophys. Res.*, *114*(A1), A01,202–, 2009.

Omura, Y., N. Furuya, and D. Summers, Relativistic turning acceleration of resonant electrons by coherent whistler mode waves in a dipole magnetic field, *J. Geophys. Res.*, *112*(A6), A06,236, 2007.

Onsager, T. G., J. C. Green, G. D. Reeves, and H. J. Singer, Solar wind and magnetospheric conditions leading to the abrupt loss of outer radiation belt electrons, *J. Geophys. Res.*, *112*(A1), A01,202–, 2007.

Otto, A., and D. H. Fairfield, Kelvin-helmholtz instability at the magnetotail boundary: Mhd simulation and comparison with geotail observations, *J. Geophys. Res.*, *105*(A9), 21,175–21,190, 2000.

Paulikas, G. A., and J. B. Blake, Effects of the solar wind on magnetospheric dynamics: Energetic electrons at the synchronous orbit, *Quantitative Modeling of Magnetospheric Processes, Geophys. Monogr. Ser.*, *21*, 180–202, aGU, Washington, D. C., 1979.

Qin, Z., R. E. Denton, N. A. Tsyganenko, and S. Wolf, Solar wind parameters for magnetospheric magnetic field modeling, *Space Weather*, *5*(11), S11,003–, 2007.

Reeves, G. D., Relativistic electrons and magnetic storms: 1992-1995, *Geophys. Res. Lett.*, *25*(11), 1817–1820, 1998.

Reeves, G. D., K. L. McAdams, R. H. W. Friedel, and T. P. O'Brien, Acceleration and loss of relativistic electrons during geomagnetic storms, *Geophys. Res. Lett.*, *30*(10), 1529, 2003.

Reeves, G. D., A. Chan, and C. Rodger, New directions for radiation belt research, *Space Weather*, *7*(7), S07,004, 2009.

Reeves, G. D., S. K. Morley, R. H. W. Friedel, M. G. Henderson, T. E. Cayton, G. Cunningham, J. B. Blake, R. A. Christensen, and D. Thomsen, On the relationship between relativistic electron flux and solar wind velocity: Paulikas and blake revisited, *J. Geophys. Res.*, *116*(A2), A02,213, 2011.

Rostoker, G., S. Skone, and D. N. Baker, On the origin of relativistic electrons in the magnetosphere associated with some geomagnetic storms, *Geophys. Res. Lett.*, *25*(19), 3701–3704, 1998.

Russell, C. T., and R. L. McPherron, Semiannual variation of geomagnetic activity, *J. Geophys. Res.*, *78*(1), 92–108, 1973.

Schulz, M., and L. J. Lanzerotti, *Particle diffusion in the radiation belts*, Physics and Chemistry in Space, Berlin: Springer, 1974.

Sheldon, R. B., H. E. Spence, J. D. Sullivan, T. A. Fritz, and J. Chen, The discovery of trapped energetic electrons in the outer cusp, *Geophys. Res. Lett.*, *25*(11), 1825–1828, 1998.

Shprits, Y. Y., D. A. Subbotin, N. P. Meredith, and S. R. Elkington, Review of modeling of losses and sources of relativistic electrons in the outer radiation belt ii: Local acceleration and loss, *Journal of Atmospheric and Solar-Terrestrial Physics*, *70*(14), 1694–1713, 2008.

Shue, J.-H., J. K. Chao, H. C. Fu, C. T. Russell, P. Song, K. K. Khurana, and H. J. Singer, A new functional form to study the solar wind control of the magnetopause size and shape, *J. Geophys. Res.*, *102*(A5), 9497–9511, 1997.

Summers, D., and R. M. Thorne, Relativistic electron pitch-angle scattering by electromagnetic ion cyclotron waves during geomagnetic storms, *J. Geophys. Res.*, *108*(A4), 1143, 2003.

Summers, D., R. M. Thorne, and F. Xiao, Relativistic theory of wave-particle resonant diffusion with application to electron acceleration in the magnetosphere, *J. Geophys. Res.*, *103*(A9), 20,487–20,500, 1998.

Summers, D., C. Ma, N. P. Meredith, R. B. Horne, R. M. Thorne, D. Heynderickx, and R. R. Anderson, Model of the energization of outer-zone electrons by whistler-mode chorus during the october 9, 1990 geomagnetic storm, *Geophys. Res. Lett.*, *29*(24), 2174, 2002.

Summers, D., C. Ma, N. Meredith, R. Horne, R. Thorne, and R. Anderson, Modeling outer-zone relativistic electron response to whistler-mode chorus activity during substorms, *Journal of Atmospheric and Solar-Terrestrial Physics*, *66*(2), 133–146, 2004.

Figure 1. A log-log plot showing the energy of the electron flux E, against the effective time delay of the solar wind velocity τ calculated from the NARMAX results.

Figure 2. The velocity in black and the log of the electron flux, J, for energies 24.1 keV (blue), 270 keV (red) and 925 keV (green), starting on the 21^{st} February 2004 and ending on the 6^{th} March 2004.

Figure 3. The scatter plots of (a) the current day's solar wind velocity against the current day's solar wind density, with the red points corresponding to the highest 5% of the 24.1 keV electron flux (greater than $10^{5.6}(\mathrm{cm}^3\cdot\mathrm{s}\cdot\mathrm{sr}\cdot\mathrm{keV})^{-1}$). (b) the current day's solar wind velocity against the previous day's solar wind density, with the red points corresponding to the highest 5% of the 24.1 keV electron flux (greater than $10^{5.6}(\mathrm{cm}^3\cdot\mathrm{s}\cdot\mathrm{sr}\cdot\mathrm{keV})^{-1}$). (c) the solar wind velocity from two day's in the past against the previous day's solar wind density, with the red points corresponding to the highest 5% of the 1.8-3.5 MeV electron flux (greater than $10^{0.76}(\mathrm{cm}^3\cdot\mathrm{s}\cdot\mathrm{sr}\cdot\mathrm{keV})^{-1}$).

Temerin, M., and X. Li, Dst model for 1995 - 2002, *J. Geophys. Res.*, *111*(A4), A04,221, 2006.

Temerin, M., I. Roth, M. Hudson, and J. Wygant, New paradigm for the transport and energization of radiation belt particles, *Eos Trans. AGU*, *75*, 538, 1994.

Van Allen, J. A., The geomagnetically trapped corpuscular radiation, *J. Geophys. Res.*, *64*(11), 1683–1689, 1959.

Wei, H., S. Billings, and J. Lui, Term and variable selection for nonlinear models, *Int. Control J.*, *77*, 86–110, 2004.

$J_{24.1k}$, 24.1keV

Term	**ERR (%)**	**Selected**
$V(t)$	96.928	8
$V^2(t)$	2.824	8
$n(t)$	0.082	8
$B_z(t)$	0.041	5
$VB_z(t)$	0.027	3

$J_{31.7k}$, 31.7keV

Term	**ERR (%)**	**Selected**
$V(t)$	96.944	8
$V^2(t)$	2.825	8
$n(t)$	0.071	8
$B_z(t)$	0.037	5
$VB_z(t)$	0.025	4

$J_{41.6k}$, 41.6keV

Term	**ERR (%)**	**Selected**
$V(t)$	96.968	8
$V^2(t)$	2.819	8
$n(t)$	0.057	8
$B_z(t)$	0.033	5
$VB_z(t)$	0.022	3

$J_{62.5k}$, 62.5keV

Term	**ERR (%)**	**Selected**
$V(t)$	97.014	8
$V^2(t)$	2.798	8
$n(t)$	0.035	8
$B_z(t)$	0.028	5
$nV(t)$	0.026	6

Table 1. Results of the NARMAX analysis employing a second order nonlinearity and basic solar wind inputs. Shows the top 5 terms in the order of ERR for the electron fluxes $J_{24.1k}$ to $J_{62.5k}$

J_{90k}, 90.0keV		
Term	**ERR (%)**	**Selected**
$V(t)$	97.062	8
$V^2(t)$	2.769	8
$nV(t)$	0.026	3
$VB_z(t)$	0.019	5
$B_z(t-1)$	0.019	7

$J_{127.5k}$, 127.5keV		
Term	**ERR (%)**	**Selected**
$V(t)$	74.880	8
$V(t-1)$	22.252	7
$V^2(t)$	2.082	7
$V^2(t-1)$	0.646	7
$nV(t)$	0.020	5

$J_{172.5k}$, 172.5keV		
Term	**ERR (%)**	**Selected**
$V(t-1)$	65.687	8
$V(t)$	31.563	7
$V^2(t-1)$	1.736	8
$V^2(t)$	0.876	6
$B_z(t-1)$	0.023	7

J_{270k}, 270keV		
Term	**ERR (%)**	**Selected**
$V(t-1)$	97.476	8
$V^2(t-1)$	2.339	8
$B_z(t-1)$	0.022	7
$V(t)$	0.012	6
$pV(t)$	0.011	4

Table 2. Results of the NARMAX analysis employing a second order nonlinearity and basic solar wind inputs. Shows the top 5 terms in the order of ERR for the electron fluxes J_{90k} to J_{270k}

J_{407k}, 407.5keV		
Term	**ERR (%)**	**Selected**
$V(t-1)$	84.116	8
$V(t-2)$	13.726	4
$V^2(t-1)$	1.626	8
$V^2(t-2)$	0.247	4
$nV(t)$	0.031	4
J_{625k}, 625keV		
Term	**ERR (%)**	**Selected**
$V(t-1)$	75.876	8
$V(t-2)$	22.275	3
$V^2(t-1)$	0.610	4
$V(t-4)$	0.243	6
$V^2(t-2)$	0.215	3
J_{925k}, 925keV		
Term	**ERR (%)**	**Selected**
$V(t-2)$	96.162	8
$n(t)$	0.279	2
$V(t-4)$	0.238	7
$n(t-4)$	0.197	2
$p(t)$	0.195	4
$J_{1.3M}$, 1.3MeV		
Term	**ERR (%)**	**Selected**
$V^2(t-2)$	76.508	7
$nV(t-1)$	2.211	3
$nV(t)$	1.900	2
$V^2(t-3)$	1.692	2
$V^2(t-4)$	1.384	7

Table 3. Results of the NARMAX analysis employing a second order nonlinearity and basic solar wind inputs. Shows the top 5 terms in the order of ERR for the electron fluxes J_{407k} to $J_{1.3M}$

J_{2M}, 2.0MeV		
Term	**ERR (%)**	**Selected**
$n(t-1)$	53.692	7
$nV(t-1)$	13.561	3
$n^2(t-1)$	5.550	5
$V^2(t-4)$	4.320	5
$np(t-1)$	3.410	5
$J_{1.8-3.5M}$, 1.8 to 3.5MeV		
Term	**ERR (%)**	**Selected**
$n(t-1)$	51.504	8
$n^2(t-1)$	15.111	6
$V^2(t-2)$	6.128	7
$V^2(t-4)$	5.129	6
$pV(t-1)$	3.606	3

Table 4. Results of the NARMAX analysis employing a second order nonlinearity and basic solar wind inputs. Shows the top 5 terms in the order of ERR for the electron fluxes $J_{1.8-3.5M}$ and $J_{1.8-3.5M}$

Figure 4. Panel (a) displays, for each velocity, the probability of a top 5% 1.8-3.5 MeV electron flux occurring at a particular density. Panel (b) shows, for each velocity, the probability of a particular density occurring.

Figure 5. The 1 minute solar wind velocity (blue), 1 minute density (red) and 1 minute dynamic pressure (magenta), with the daily log of the electron fluxes (black) for the energies 1.8-3.5 MeV (d), 625 keV (e) and 270 keV (f). Panel (g) shows the 1 minute magnetopause location along the Earth-Sun according to the *Shue et al.* [1997]. Starting on the 7th November 2000 and ending on the 1st December 2000.

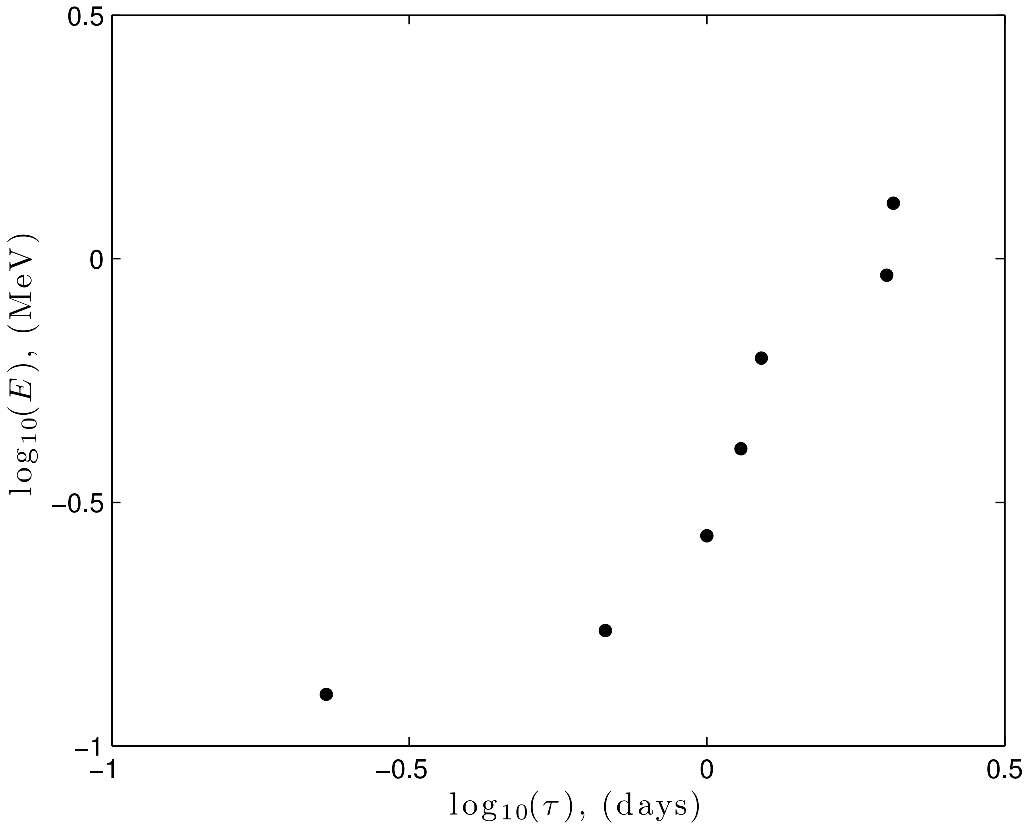
0.5
0
−0.5
−1
−1
−0.5
0
0.5
$\log_{10}(E)$, (MeV)
$\log_{10}(\tau)$, (days)

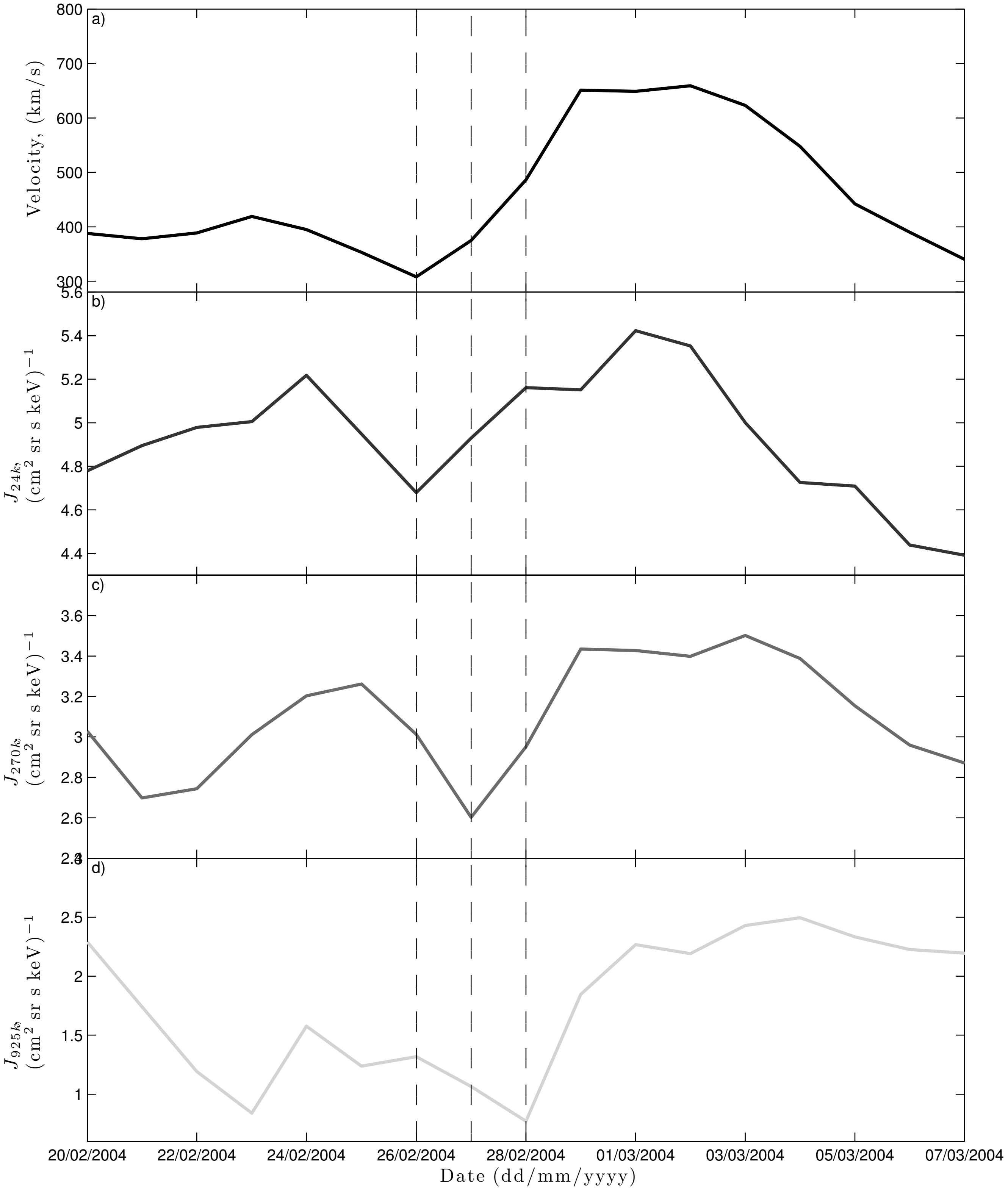
a)
b)
c)
d)
Velocity, (km/s)
800
700
600
500
400
300
J_{24k}, $(\mathrm{cm}^2\ \mathrm{sr\ s\ keV})^{-1}$
5.6
5.4
5.2
5
4.8
4.6
4.4
J_{270k}, $(\mathrm{cm}^2\ \mathrm{sr\ s\ keV})^{-1}$
3.6
3.4
3.2
3
2.8
2.6
2.4
J_{925k}, $(\mathrm{cm}^2\ \mathrm{sr\ s\ keV})^{-1}$
3
2.5
2
1.5
1
20/02/2004
22/02/2004
24/02/2004
26/02/2004
28/02/2004
01/03/2004
03/03/2004
05/03/2004
07/03/2004
Date (dd/mm/yyyy)

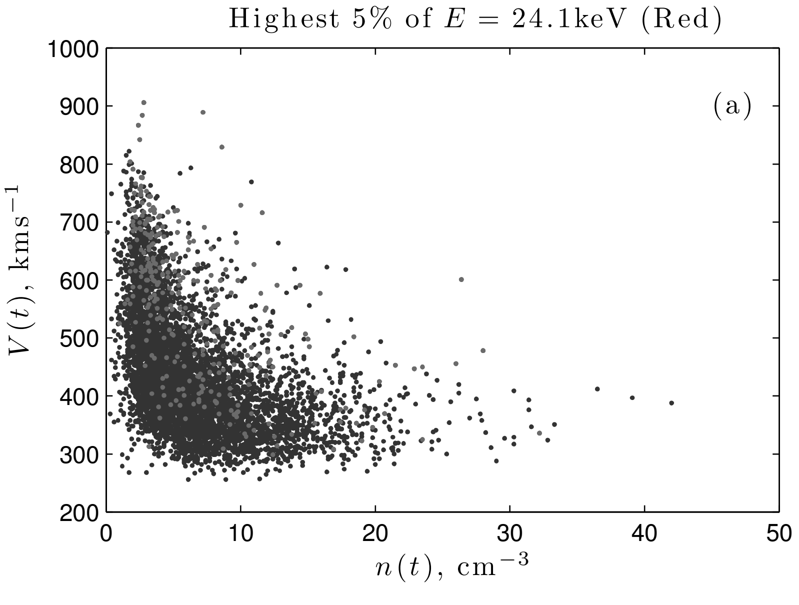
Highest 5% of $E = 24.1$keV (Red)

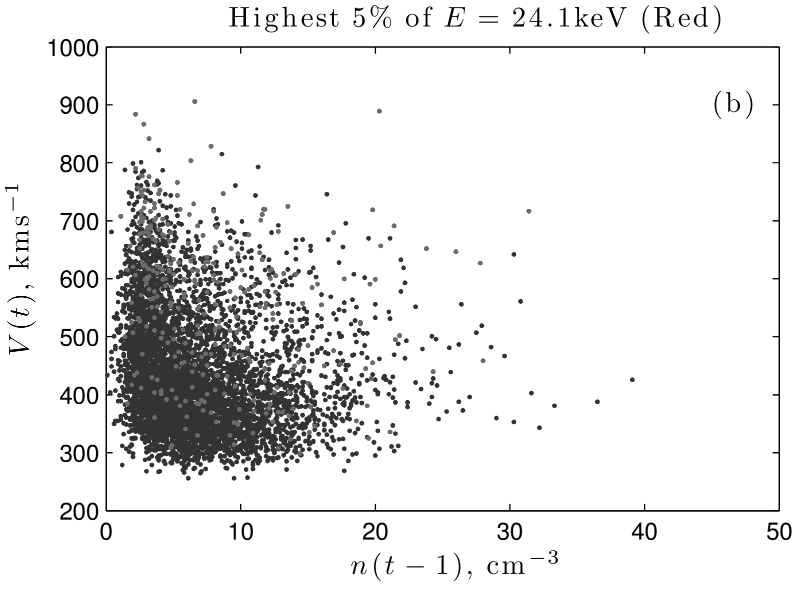
Highest 5% of $E = 24.1$keV (Red)

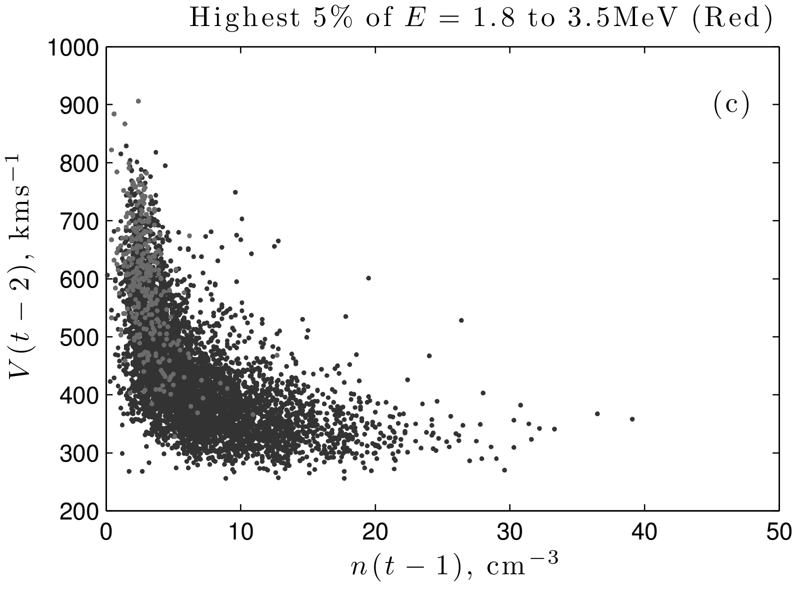
Highest 5% of $E = 1.8$ to 3.5MeV (Red)

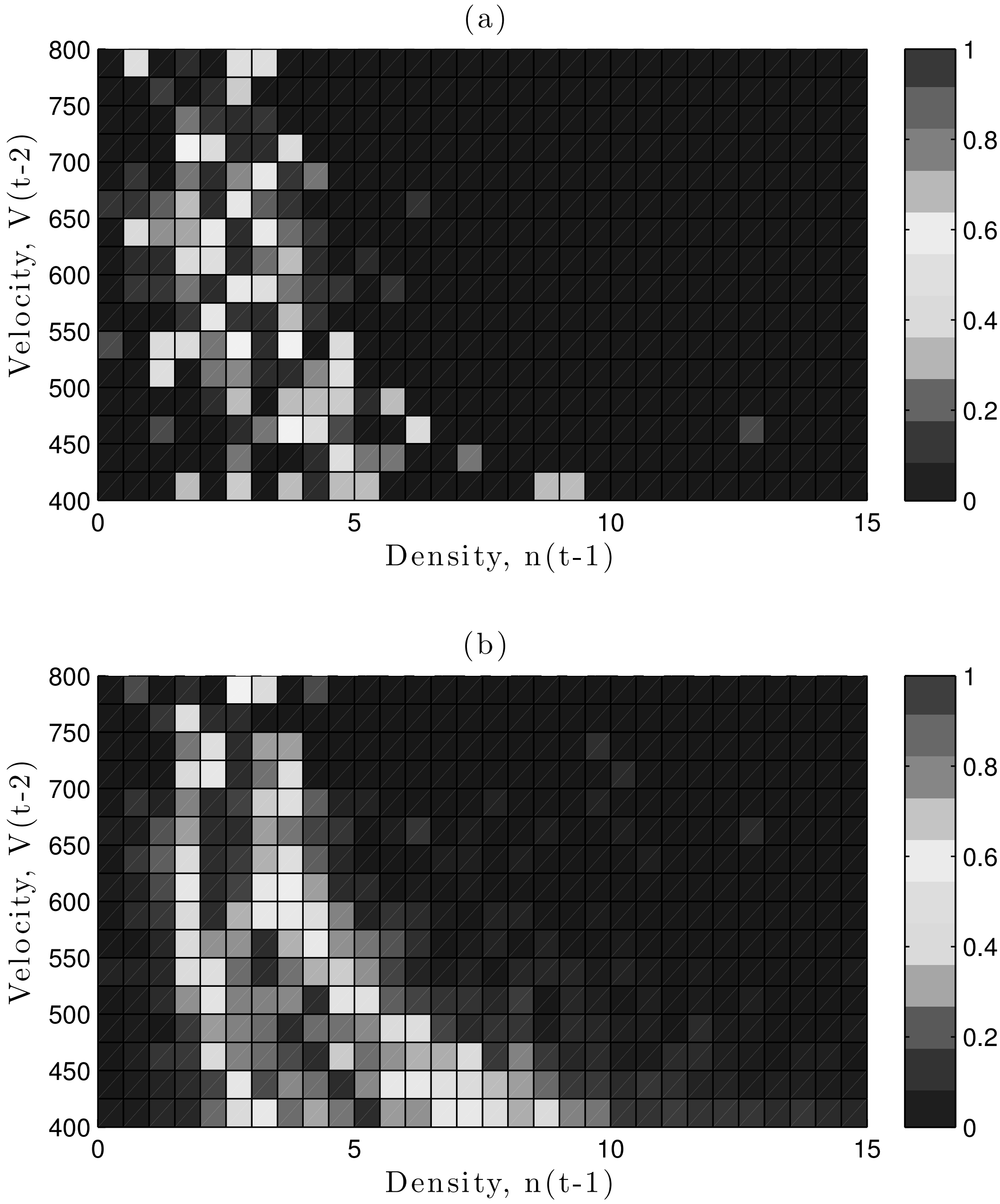
(a)
800
750
700
650
600
550
500
450
400
Velocity, V(t-2)
0
5
10
15
Density, n(t-1)
1
0.8
0.6
0.4
0.2
0
(b)
800
750
700
650
600
550
500
450
400
Velocity, V(t-2)
0
5
10
15
Density, n(t-1)
1
0.8
0.6
0.4
0.2
0

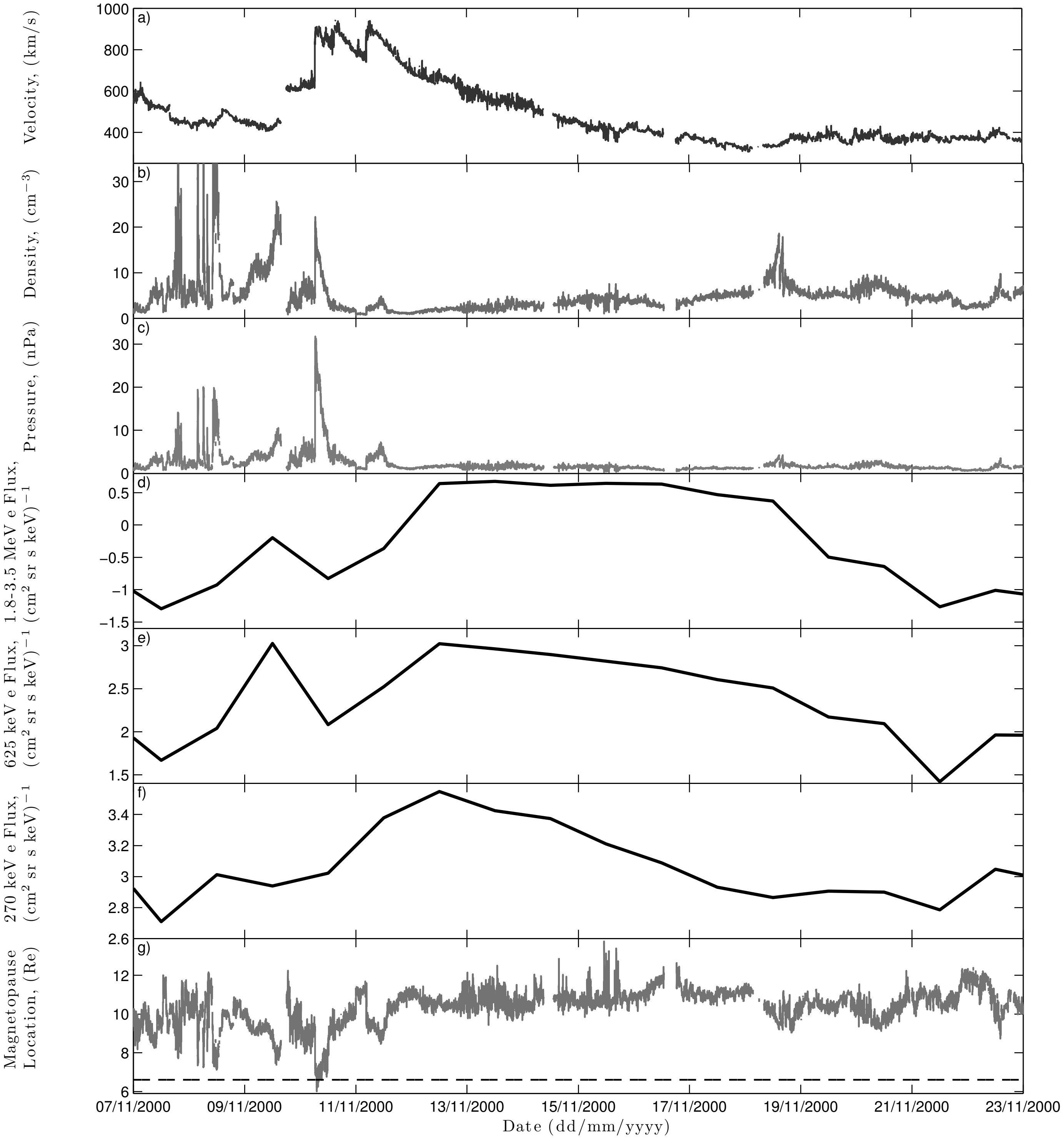
a)
Velocity, (km/s)
1000
800
600
400
b)
Density, (cm^{-3})
30
20
10
0
c)
Pressure, (nPa)
30
20
10
0
d)
1.8-3.5 MeV e Flux, $(\mathrm{cm}^2\ \mathrm{sr\ s\ keV})^{-1}$
0.5
0
−0.5
−1
−1.5
e)
625 keV e Flux, $(\mathrm{cm}^2\ \mathrm{sr\ s\ keV})^{-1}$
3
2.5
2
1.5
f)
270 keV e Flux, $(\mathrm{cm}^2\ \mathrm{sr\ s\ keV})^{-1}$
3.4
3.2
3
2.8
2.6
g)
Magnetopause Location, (Re)
12
10
8
6
07/11/2000
09/11/2000
11/11/2000
13/11/2000
15/11/2000
17/11/2000
19/11/2000
21/11/2000
23/11/2000
Date (dd/mm/yyyy)